Atmos. Chem. Phys. Discuss., 11, 11839–11859, 2011
www.atmos-chem-phys-discuss.net/11/11839/2011/
doi:10.5194/acpd-11-11839-2011

Atmospheric Chemistry and Physics Discussions

The observation of chemiluminescent NiO^* emissions in the laboratory and in the night airglow

W. F. J. Evans[1,2], R. L. Gattinger[3], A. L. Broadfoot[4], and E. J. Llewellyn[3]

[1]NorthWest Research Associates Inc., 4118 148 Avenue N.E., Redmond WA 98052, USA
[2]Centre for Research in Experimental Space Science, York University, 4700 Keele Street, Toronto, ON M3J 1P3, Canada
[3]ISAS, Department of Physics and Engineering Physics, 116 Science Place, University of Saskatchewan, Saskatoon SK S7N 5E2, Canada
[4]Lunar and Planetary Laboratory, University of Arizona, 1629 E. University Blvd., Tucson AZ 85721-0092, USA

Received: 18 March 2011 – Accepted: 26 March 2011 – Published: 15 April 2011

Correspondence to: W. F. J. Evans (edward.llewellyn@usask.ca)

Published by Copernicus Publications on behalf of the European Geosciences Union.

Abstract

The recent finding of an orange spectral feature in OSIRIS/Odin spectra of the night airglow near 85 km has raised interest in the origin of the emission. The feature was positively identified as the chemiluminescent FeO^* emission where the iron is of meteoric origin. Since the meteorite source of atomic metals in the mesosphere contains both iron and nickel, with Ni being typically 6% of Fe, it is expected that faint emissions involving Ni should also be present in the night airglow. The present study summarizes the laboratory observations of chemiluminescent NiO^* emissions and includes a search for the NiO^* signature in the night airglow. A faint previously unidentified "continuum" extending longwave of 440 nm has been identified in night airglow spectra obtained with two space-borne limb viewing instruments and through a comparison with laboratory spectra this continuum is identified as arising from the NiO^* emission. The FeO^* and NiO^* emissions both originate from a reaction of the metal atoms with mesospheric ozone and so support the presence of NiO^* in the night airglow.

1 Introduction

The terrestrial night airglow has been studied for more than a century (e.g. Ångström, 1869). However, new emission features, most recently the FeO "orange" bands that arise from the reaction between atomic iron of meteoric origin with ozone, are still being identified (Evans et al., 2010). Known emission features continue to be investigated and their spectral signatures more accurately determined; one example is the chemiluminescent emission of NO_2^* that is produced in the NO+O reaction (Gattinger et al., 2010). Extending these ongoing observations, it is expected that a chemiluminescent emission from NiO^*, which also arises from the reaction of atomic nickel of meteoric origin (McNeil et al., 1998) with atmospheric ozone, should be present in the airglow spectrum, albeit very faint.

ACPD
11, 11839–11859, 2011

At least two NiO* band systems are known to be present in the visible spectral region, the NiO "blue" bands in the 500 nm region (Srdanov and Harris, 1988) and the "red" $^3\Sigma^- - X\ ^3\Sigma^-$ system that occurs in the 620 nm region (Friedman-Hill and Field, 1992). Due to the complexity of the spectra the determination of the molecular constants for the upper electronic states is challenging and consequently the definitive assignment of vibrational transitions remains incomplete. Srdanov and Harris (1988) did publish a laboratory spectrum of chemiluminescent NiO* over the 480 to 600 nm wavelength range and more recently Burgard et al. (2006) obtained the spectrum over a much broader wavelength range, although at much lower spectral resolution. In the present study the NiO* spectra observed in the laboratory are summarized and discussed. In addition, a preliminary spectral model of the NiO* emissions is introduced, primarily to investigate the probable change in spectral shape when transferring the NiO* laboratory spectra, obtained at relatively high pressure, to the much lower pressures associated with the mesopause region.

Night airglow spectra recorded by two limb-viewing space-borne spectrographs on separate platforms are presented. The airglow spectra are corrected for atomic emissions and for the well-known molecular emission systems, mainly the Herzberg O_2 bands in the near-ultraviolet and blue regions, and the Meinel hydroxyl bands in the red spectral region. The residual observed spectra are then compared with the laboratory observations of the NiO* band systems.

2 Laboratory observations of the chemiluminescent NiO* emission

The earliest observations of the NiO* emissions were recorded by Rosen (1945) who identified numerous spectral features and proposed a band classification scheme. Srdanov and Harris (1988) applied high resolution spectroscopic techniques to study the emissions in greater detail. These latter authors observed additional spectral features and proposed changes to the earlier band classifications. From a detailed spectral analysis Friedman-Hill and Field (1992) obtained accurate molecular constants for the NiO ground state and identified another NiO band system in the one micron region.

ACPD
11, 11839–11859, 2011

Balfour et al. (2004) simplified the emission spectrum by cooling the emission source via an expansion jet and were able to identify additional bands, particularly those arising from the lowest ground state energy level. The observed rotationally resolved band spectra form a basic part of the spectral model referred to below.

The dominant chemical reaction that produces NiO^* in the mesopause region is expected to be

$$Ni + O_3 \rightarrow NiO^* + O_2(+266 \pm 4\,kJ\,mol^{-1}) \quad (R1)$$

With a bond energy for NiO of $373 \pm 3\,kJ\,mol^{-1}$ (Watson et al., 1993), the upper energy limit for the NiO^* product is approximately $22\,600\,cm^{-1}$, or 440 nm. This limit is in agreement with the laboratory observations of Burgard et al. (2006) (Fig. 1). The laboratory spectrum has been converted to photon units to compare with the space-borne observations discussed in the next section.

An independent laboratory spectrum of chemiluminescent NiO^* arising from the $Ni + O_3$ reaction was obtained by Srdanov and Harris (1988). The spectral range extends from approximately 480 nm to 600 nm (Fig. 1) and the spectral resolution is considerably higher than for the Burgard et al. (2006) spectrum of NiO^*. The two observed spectra in Fig. 1 form the basis of a "reference" NiO^* spectrum used in the following sections to search for the presence of the NiO^* spectral signature in the night airglow.

A preliminary spectral model of the NiO^* bands is also included in Fig. 1. This model spectrum has been convolved with a slit function for an approximate match to the resolution of the Burgard et al. (2006) spectrum. The model will be described in detail elsewhere and because some of the spectroscopic constants required to produce an accurate model are unavailable it must be stressed that the model is preliminary. The primary function of the model in this study is to relate the laboratory NiO^* observations made at relatively high pressures to the much lower pressure regime in the mesopause region. A similar study involving FeO^* observations in the laboratory and in the airglow (Gattinger et al., 2011) determined that the higher vibrational levels in the airglow are more heavily populated than those in the higher pressure laboratory observations. Accordingly, for the comparison with laboratory spectra in Fig. 1 the lower vibrational

ACPD
11, 11839–11859, 2011

levels in the excited NiO^* states are assumed to be more heavily populated than the upper levels. With this assumption most of the prominent features observed in the two laboratory spectra are matched by the model spectrum. The calculated Franck-Condon factors for the band systems included in the model must also be considered preliminary due to the lack of accurate spectroscopic constants. Although individual relative band intensities will change with more accurate Franck-Condon factors it is expected that the overall distribution will remain similar and so have only a minor impact on the conclusions of the present study.

At instrumental resolutions typical for very faint airglow observations the spectrum in Fig. 1 will appear as a pseudo-continuum. This "continuum" is expected to be very faint, thus making it difficult to detect in ground-based airglow spectra, which necessarily contain a strong non-atmospheric component (Sternberg and Ingham, 1972). Consequently, data obtained with limb-viewing space-borne spectrographs are better suited to the task because of the airglow limb enhancement factor of at least fifty relative to the non-atmospheric background. A search for a spectral signature in the night airglow that matches the chemiluminescent NiO^* "continuum" is described in the following sections.

3 Night airglow continuum observations with the GLO-1 spectrograph

Limb-viewing spectra from the Arizona GLO-1 imaging spectrograph (Broadfoot et al., 1992) are described here as part of the search for the NiO^* signature in the night airglow. The GLO-1 instrument is a Space Shuttle-borne optical suite that included an imaging spectrograph with a spectral range from 120 to 900 nm and a spectral resolution that ranges from 0.5 nm to 1 nm. In the current analysis the averaged GLO-1 night airglow tangent limb spectrum, shown in Panel A of Fig. 2, was obtained on mission STS 53 that flew 2–12 December 1992 (Broadfoot and Bellaire, 1999). Other spectra from this instrument have been used to study meteoric metals in the thermosphere (Gardener et al., 1999).

ACPD
11, 11839–11859, 2011

Following the procedures described by Evans et al. (2010), known airglow emission features were matched to the observed spectrum. These features included the Herzberg O_2 band systems, the Meinel OH bands, the O_2 Atmospheric bands and a number of atomic emission lines. The assembled matching simulated spectrum is shown in Panel B of Fig. 2. This model spectrum has been subtracted from the observed spectrum of Panel A to give the difference spectrum that is shown in Panel C of Fig. 2. This spectrum includes the "unidentified" features present in the GLO-1 night airglow spectrum. It is apparent from Panel C that the spectral region from 380 to 430 nm contains a continuum that is nearly uniform, with a tangent limb brightness of approximately 3×10^7 photons cm^{-2} s^{-1} nm^{-1}. Converted to an equivalent zenith viewing brightness this is less than 10^6 photons cm^{-2} s^{-1} nm^{-1}, or less than 1/10 Rayleigh $Å^{-1}$. This is close to an order of magnitude fainter than the ground-based continuum brightness observed by Broadfoot and Kendall (1968), and underlines the difficulty of searching for very faint continuum sources in ground-based spectra.

The residual "continuum" spectrum in Panel C of Fig. 2 shows a clear increase in brightness with increasing wavelength from 440 nm to 550 nm. Also included for comparison in this figure is the known spectral shape of the NO + O reaction that produces chemiluminescent NO_2^* (Gattinger et al., 2009). The increase between 450 nm and 550 nm observed in the GLO-1 spectrum does not match the spectral shape of the NO_2^* emission. In addition Gattinger et al. (2010) found that at latitudes equatorward of 40^o the NO_2^* signature is very faint relative to the more poleward night airglow NO_2^* brightness. The model spectral profile of chemiluminescent FeO^* at mesospheric altitudes (Gattinger et al., 2011), shown in Panel C for reference, is required in the analysis to account for the expected spectral contribution from FeO^* emission (Evans et al., 2010).

In Fig. 3 the residual continuum observed by the GLO-1 instrument (Panel C of Fig. 2) is compared with the NiO^* model spectrum for laboratory pressure (Fig. 1) and the chemiluminescent NiO^* model spectrum computed for mesospheric pressures. The spectral region beyond 620 nm has been omitted in order to stress the blue region. An average of the observed unexplained nearly uniform continuum between 380 nm to

ACPD
11, 11839–11859, 2011

430 nm, approximately 3×10^7 photons cm^{-2} s^{-1} nm^{-1}, has been subtracted from the residual spectrum over the whole wavelength range. The mesospheric NiO^* model spectrum threshold in the 450 nm region is located to the blue by approximately 20 nm compared with the model spectrum for laboratory pressure. This is in agreement with the blue threshold of the observed GLO-1 spectrum.

It is apparent from Fig. 3 that the model NiO^* spectrum for laboratory pressures is quite different from the NiO^* model spectrum for mesospheric pressures. To confirm this difference new laboratory measurements and detailed analyses are required to determine accurate spectroscopic parameters. In the present analysis, a wedge distribution (linear weights from 1 to 10) of vibrational level populations has been assumed for the laboratory pressures. A flat distribution of equal weights has been used to simulate the vibrational distribution at mesospheric pressures levels appropriate to the satellite observations. In the future, valuable information could be obtained from rocket releases into the mesosphere that generate NiO^* vapour trails using techniques similar to those employed by Best et al. (1972) to generate FeO^* emissions.

Following the observations of Evans et al. (2010), the residual GLO-1 spectrum in Fig. 2, Panel C, is expected to include a component arising from mesospheric chemiluminescent FeO^* emissions. The Evans et al. (2010) study is built on the observation of FeO^* in persistent meteor trains by Jenniskens et al. (2000). The FeO^* component must be removed from the total residual continuum to isolate any previously unidentified features. A least squares combination of the model mesospheric FeO^* and NiO^* spectral profiles, applied to the GLO-1 residual continuum, is shown in Fig. 4. The spectral region above 670 nm is omitted in order to avoid the excessive noise in the difference spectrum caused by the stronger OH bands towards the infrared. The NiO^* to FeO^* ratio, summed over the spectral region of Fig. 4, is 3.2 ± 0.4 as derived from the least squares procedure. The model threshold at 450 nm is in good agreement with the observed threshold. Again, it must be stressed that the model simulations are preliminary versions.

ACPD
11, 11839–11859, 2011

The mesospheric model spectrum in Fig. 4 contains features at 455 nm and 470 nm that correspond to transitions arising from upper levels centred on $v' = 5$ of the upper electronic state of the "blue" NiO^* band system. These relatively high vibrational levels observed in the airglow are in accord with the premise that NiO^* is excited to high vibrational levels at mesospheric pressures. The brightness of the bands towards the blue is constrained by the decreasing Franck-Condon factors for bands with larger vibrational quantum differences.

4 Night airglow continuum observations with the OSIRIS spectrograph

An analysis similar to that presented in the preceding section was completed for selected tangent limb night airglow observations made with the space-borne OSIRIS spectrograph (Llewellyn et at., 2004). The OSIRIS spectral range is from 274 nm to 815 nm with a spectral resolution of approximately 1 nm. Individual spectra, recorded as the bore-sight repetitively scans the limb, are averaged over both tangent limb altitude and elapsed time to improve signal-to-noise. An example of an average spectrum for the June and July, 2004 observing period is shown in Panel A of Fig. 5. As in Fig. 2 for the GLO-1 observations, the matching simulated spectrum of the known airglow features, scaled to the observed OSIRIS average spectrum, is shown in Panel B of Fig. 5. The difference between the observed spectrum in Panel A and the simulated spectrum in Panel B is shown in Panel C of Fig. 5. This residual spectrum includes the "unidentified" features present in the OSIRIS night airglow spectrum.

It is apparent that the OSIRIS residual "continuum" spectrum (Panel C of Fig. 5) differs in spectral shape from the GLO-1 residual continuum shown in Panel C of Fig. 2. In particular the component arising from the FeO^* chemiluminescent emission appears to be brighter in the OSIRIS spectrum. This is addressed in a quantitative manner in Fig. 6 where a least-squares fitting of the mesospheric models of the NiO^* and FeO^* spectral profiles is applied to resolve the two components present in the OSIRIS spectrum, as in Fig. 4 for the GLO-1 analysis. The NiO^* to FeO^* ratio is 0.3 ± 0.1,

ACPD
11, 11839–11859, 2011

integrated over the full spectral range of Fig. 6 as determined from the least squares fitting procedure.

Additional OSIRIS observing periods are discussed here in an attempt to investigate the variability of the observed NiO^* to FeO^* ratio. For the April and May 2003 period (see Evans et al., 2010) a ratio of 0.1 ± 0.05 is obtained. For the June and July periods from 2003 to 2008 a ratio ranging from 0.0 to 0.5 is obtained from the least squares fit. This variability is discussed in the next section.

5 Chemiluminescent NiO^* and FeO^* emission sources and observed variability

Since both nickel oxide and iron oxide emissions are excited in the laboratory by chemiluminescent reactions with ozone, and both metals have their source in meteorites, it is expected that NiO would be an emission feature in the night airglow. In addition the similarity of the altitude of the detected continuum emission with the altitude distribution of the FeO band emission, indicates that the feature should be due to chemiluminescent excitation involving ozone reactions. Indeed, the reaction cycle for NiO excitation is similar to the Fe excitation cycle:

$$Ni + O_3 \rightarrow O_2 + NiO^* \quad \text{(R2)}$$

followed by

$$NiO + O \rightarrow Ni + O_2 \quad \text{(R3)}$$

Like iron, the nickel atom is recycled and catalytically enhances the conversion of odd oxygen into O_2. Typical altitude profiles of atomic iron have been determined with LIDAR measurements (Kane and Gardner, 1993a). The unidentified "continuum" emissions described here emanate from the same altitude region. Thus the chemistry itself supports the thesis that the emission feature is due to NiO^*.

The analysis of the NiO^*/FeO^* ratio by the least squares method above has been successful in deriving the individual emission intensities of FeO^* and NiO^* from a number of spectra. There is considerable variability in the observed NiO^* to FeO^* emission

ACPD
11, 11839–11859, 2011

ratio in the night airglow. Summarizing from the previous sections, the GLO-1 spectrum (Fig. 4) indicates an NiO^* to FeO^* ratio of approximately 3:1 while for the OSIRIS spectrum (Fig. 6) a ratio of approximately 1:3 is obtained. The OSIRIS spectrum for April and May of 2003 (Evans et al., 2010) indicates a ratio less than 0.1 with an obvious enhancement of FeO^* in the spectrum. While the OSIRIS night airglow spectra always exhibit a detectable FeO^* emission, on occasion there is no detectable NiO^* emission. While we have no explanation for this ratio variation it is most likely due to the variability of the meteoritic metal influx ratios.

The GLO-1 spectrum shown in Fig. 4 was taken during the period from 2–11 December 1992. This immediately precedes the maximum of the GEMINID meteor shower, which is centered on 13 December (Lokanadham et al., 2010), and follows the Leonids shower of 17 November, a shower with highly variable rates (Brown, 1999) with a periodicity of 33 yr. The OSIRIS spectrum shown in Fig. 6 was taken during June–July, 2004, well removed from the December period. The April and May observing period includes the Lyrids meteor shower that is centered on 22 April (Observer's Handbook, 2011).

There are two sources of atmospheric nickel from meteorites, ablation of meteors and sedimentation of cosmic dust (Hemenway and Hallgren, 1970). The different sources of meteoritic metals has been reviewed by Rietmeijer (2000). Ablation from meteors maximizes between 85 km and 90 km (Kane and Gardner, 1993b), at times from meteors that have high Ni/Fe ratios (Schramm et al., 1989) that originate from the cores of planetoids, the annual Leonids shower in November is one example. Taenite (Fe, Ni) is a mineral found naturally on Earth mostly in iron meteorites (Albertson et al., 1978); it is an alloy of iron and nickel with nickel proportions ranging from 20% up to as high as 65%. Typically, most meteorites have lower Ni/Fe ratios, around 8% (Brown and Patterson, 1947). The variability in meteor Ni/Fe ratios might explain some of the observed variation in the observed NiO^* to FeO^* ratios. The elemental composition analysis of 200 samples of stratospheric dust (Jessberger et al., 2001) indicated that the ratio of atomic Ni/Fe in cosmic dust is near 80%. In addition there is the complex

ACPD
11, 11839–11859, 2011

altitude distribution of mesospheric and thermospheric metals that arise from meteor deposition (Gardner et al., 1999). The profiles of Fe^+ measured with mass spectrometers on rocket flights suggest that the sedimentation cosmic dust source is significant from 80 to above 120 km (Grebowsky and Aikin, 2002). This is further supported by lidar measurements of atomic sodium, which demonstrate an ablation profile superimposed on a much broader altitude background profile (Lokanadham et al., 2010).

Another possible reason for the NiO^* to FeO^* ratio variability might be differences in mesospheric excitation processes. West and Broida (1975) estimated a 2% to 6% production efficiency of FeO^* from $Fe + O_3$. Extrapolating their laboratory measurements taken at two relatively high pressures to the much lower mesospheric pressures suggests that this efficiency could increase considerably above 6%. Currently there does not appear to be an equivalent measurement of the NiO^* production efficiency. If it is assumed that the efficiency for NiO^* production in the reaction of Ni with O_3 is higher than the efficiency for the production of FeO^* by a factor of 5, then the ratios become 3:5, 1:50 and 1:16 respectively for the abundances of atomic Ni and Fe in the three spectra; GLO 1992, OSIRIS 2004 and OSIRIS 2003. For each of the June and July periods from 2003 to 2008, the Ni/Fe ratio could vary from 0:1 to 1:10. By way of comparison with atomic ratios of Ni/Fe measured in fallen meteorites, the ratio of 3:5 for the GLO spectrum is consistent with the observed ratio of up to 80% in some meteorites. The ratio of 1:16 from OSIRIS 2003 is consistent with the observed meteorite ratio of 6%.

6 Summary

The discovery of a chemiluminescent FeO^* emission feature in OSIRIS/Odin spectra of the night airglow near 87 km has raised interest in other meteorite metallic emissions in the airglow. Since the meteorite source of atomic metals in the mesosphere contains both iron and atomic nickel, with Ni being typically 6% of Fe, it is expected that faint emissions involving Ni should also be present in the night airglow. A new spectral

ACPD
11, 11839–11859, 2011

model has been used to model the laboratory observations of chemiluminescent NiO^* emissions and then to search for the signature of NiO^* in satellite measurements of the night airglow. A faint, previously unidentified, "continuum" extending longwave of 440 nm has been identified in night airglow spectra obtained from two space-borne limb viewing instruments. From a comparison with laboratory spectra this continuum is identified as arising from the NiO^* emission generated in the ozone and atomic nickel reaction. The observation that FeO^* and NiO^* emissions both originate from a reaction with mesospheric ozone lends support to the postulated explanation of the presence of NiO^* in the night airglow. A simultaneous least-squares fit for NiO^* and FeO^* spectral profiles was conducted on Shuttle GLO and OSIRIS satellite observations of visible airglow spectra. The observed ratio of NiO^*/FeO^* is 3.2 from the GLO experiment and 0.3 in an OSIRIS observation. From the presented analysis it is suggested that the luminous efficiency of the reaction of atomic Ni with ozone is five times greater than the luminous efficiency for the atomic Fe reaction with ozone in order to yield model results that are consistent with the observation that the ratio of nickel/iron is always less than 90% in all meteorite measurements. The presented space-borne observations indicate that the Ni/FeO atomic ratio is quite variable, 64% and 6% for the two occasions of the analyzed observations.

Acknowledgements. This work was supported by the Canadian Space Agency and the Natural Sciences and Engineering Research Council (Canada). Odin is a Swedish-led satellite project funded jointly by Sweden (SNSB), Canada (CSA), France (CNES) and Finland (Tekes). Funding for the Shuttle flight and the GLO-1 instrument came from NASA and USAF Phillips Laboratory.

References

Albertsen, F., Knudsen, J. M., and Jensen, G. B.: Structure of taenite in two iron meteorites, Nature, 273, 453–454, 1978.

Ångström, A. J.: Spektrum des nordlichts, Pogg. Ann., 137, 161–163, 1869.

Balfour, W. J., Cao, J., Jensen, R. H., and Li, R.: The spectrum of nickel monoxide between 410 and 510 nm: laser-induced fluorescence and dispersed fluorescence measurements, Chem. Phys. Lett., 385, 239–243, 2004.

Best, G. T., Forsberg, C. A., Golomb, D., Rosenberg, N. W., and Vickery, W. K.: The release of iron carbonyl into the upper atmosphere, J. Geophys. Res., 77, 1677–1680, 1972.

Broadfoot, A. L. and Bellaire, P. J.: Bridging the gap between ground-based and space-based observations of the night airglow, J. Geophys. Res., 104, 17127–17138, 1999.

Broadfoot, A. L. and Kendall, K. R.: The airglow spectrum, 3100–10 000 Å, J. Geophys. Res., 73, 426–428, 1968.

Broadfoot, A. L., Sandel, B. R., Knecht, D., Viereck, R., and Murad, E.: A panchromatic spectrograph with supporting monochromatic imagers, Appl. Opt., 31(16), 3083–3096, 1992.

Brown, P.: The Leonid Meteor Shower: Historical Visual Observations, Icarus, 138, 287–308, 1999.

Brown, H. and Patterson, C.: The Composition of Meteoritic Matter: II. The Composition of Iron Meteorites and of the Metal Phase of Stony Meteorites, J. Geol., 55, 508–510, 1947.

Burgard, D. A., Abraham, J., Allen, A., Craft, J., Foley, W., Robinson, J., Wells, B., Xu, C., and Stedman, D. H.: Chemiluminescent reactions of nickel, iron and cobalt carbonyls with ozone, Appl. Spectrosc., 60, 99–102, 2006.

Evans, W. F. J., Gattinger, R. L., Slanger, T. G., Saran, D. V., Degenstein, D. A., and Llewellyn, E. J.: Discovery of the FeO orange bands in the terrestrial night airglow spectrum obtained with OSIRIS on the Odin spacecraft, Geophys. Res. Lett., 37, L22105, doi:10.1029/2010GL045310, 2010.

Friedman-Hill, E. J. and Field, R. W.: Analysis of the [16.0] $^3\Sigma^- - X^3\Sigma^-$ and [16.0]$^3\Sigma^-$-[4.3]$^3\Pi_i$ band systems of the NiO molecule, J. Mol. Spectrosc., 155(2), 259–276, doi:10.1016/0022-2852(92)90516-Q, 1992.

Gardner, J. A., Broadfoot, A. L., McNeil, W. J., Lai, S. T., and Murad, E.: Analysis and modeling of the GLO-1 observations of meteoric metals in the thermosphere, J. Atmos. Solar-Terr. Phys., 61, 545–562, doi:10.1016/S1364-6826(99)00013-9, 1999.

Gattinger, R. L., Evans, W. F. J., McDade, I. C., Degenstein, D. A., and Llewellyn, E. J.: Observation of the chemiluminescent NO+O→NO_2+hν reaction in the upper mesospheric dark polar regions by OSIRIS on Odin, Can. J. Phys., 87, 925–932, doi:10.1139/P09-051, 2009.

Gattinger, R. L., McDade, I. C., Alfaro Suzán, A. L., Boone, C. D., Walker, K. A., Bernath, P. F., Evans, W. F. J., Degenstein, D. A., and Llewellyn, E. J.: NO_2 air afterglow and O and NO

ACPD
11, 11839–11859, 2011

densities from Odin-OSIRIS night and ACE-FTS sunset observations in the Antarctic MLT region, J. Geophys. Res., 115, D12301, doi:10.1029/2009JD013205, 2010.
Gattinger, R. L., Evans, W. F. J., Degenstein, D. A., and Llewellyn, E. J.: A spectral model of the FeO orange bands with a comparison between a laboratory spectrum and a night airglow spectrum observed by OSIRIS on Odin., Can. J. Phys., 89, 239–248, 2011.
Grebowsky, J. M. and Aikin, A. C.: In Situ Measurements of Meteoric Ions, in: Meteors in the Earth's Atmosphere, edited by: Murat, E. and Williams, I. P., 189–214 Cambridge University Press, Cambridge, UK, 2002.
Hemenway, C. L. and Hallgren, D. S.: The Variation of the Altitude Distribution of the Cosmic Dust Layer in the Upper Atmosphere, Space Research X, 272–280, North Holland Publishing Co., Amsterdam, 1970.
Jenniskens, P., Lacey, M., Allan, B. J., Self, D. E., and Plane, J. M. C.: FeO "orange arc" emission detected in optical spectrum of Leonid persistent train, Earth, Moon and Planets, 82–83, 429–434, 2000.
Jessberger, E. K., Stephan, T., Rost, D., Arndt, P., Maetz, M., Stadermann, F. J., Brownlee, D. E., Bradley, J. P., and Kurat, G.: Properties of Interplanetary Dust: Information from Collected Samples, from the book: "Interplanetary Dust", edited by: Grün, E., Gustafson, B. Å. S., Dermott, S. F., and Fechtig, H., Springer Verlag, 509–567, 2001.
Kane, T. J. and Gardner, C. S.: Structure and seasonal variability of the nighttime mesospheric Fe layer at midlatitudes, J. Geophys. Res. 98, 16875–16886, 1993a.
Kane, T. J. and Gardner, C. S.: LIDAR observations of the meteoritic deposition of mesospheric metals, Science, 259, 1297–1300, 1993b.
Llewellyn, E. J., Lloyd, N. D., Degenstein, D. A., Gattinger, R. L., Petelina, S. V., Bourassa, A. E., Wiensz, J. T., Ivanov, E. V., McDade, I. C., Solheim, B. H., McConnell, J. C., Haley, C. S., von Savigny, C., Sioris, C. E., McLinden, C. A., Griffioen, E., Kaminski, J., Evans, W. F. J., Puckrin, E., Strong, K., Wehrle, V., Hum, R. H., Kendall, D. J. W., Matsushita, J., Murtagh, D. P., Brohede, S., Stegman, J., Witt, G., Barnes, G., Payne, W. F., Piché, L., Smith, K., Warshaw, G., Deslauniers, D.-L., Marchand, P., Richardson, E. H., King, R. A., Wevers, I., McCreath, W., Kyrölä, E., Oikarinen, L., Leppelmeier, G. W., Auvinen, H., Mégie, G., Hauchecorne, A., Lefèvre, F., de La Nöe, J., Ricaud, P., Frisk, U., Sjoberg, F., von Schéele, F., and Nordh, L.: The OSIRIS Instrument on the Odin Spacecraft, Can. J. Phys., 82, 411–422, 2004.
Lokanadham, B., Chandra, N. R., Rao, S. V. B., Raghunath, K., and Yellaiah, G.: Mesospheric

ACPD
11, 11839–11859, 2011

sodium over Gadanki during GEMINID meteor shower 2007, Indian J. Radio Space Phys., 39, 7–10, 2010.
McNeil, W. J., Lai, S. T., and Murad, E.: Differential ablation of cosmic dust and implications for the relative abundances of atmospheric metals, J. Geophys. Res., 103, 10899–10911, 1998.
Observer's Handbook: edited by: Kelly, P., Royal Astronomical Society of Canada, University of Toronto Press, 2011.
Rietmeijer, F. J. M.: Interrelationships among meteoric metals, meteors, interplanetary dust, micrometeorites, and meteorites, Meteoritics Planet. Sci., 35, 1025–1041, 2000.
Rosen, B.: Spectra of diatomic oxides by the method of exploded wire, Nature, 156, 570–570, 1945.
Schramm, L. S., Brownlee, D. E., and Wheelock, M. M.: Major element composition of stratospheric micrometeorites, Meteoritics, 24, 99–112, 1989.
Srdanov, V. I. and Harris, D. O.: Laser spectroscopy of NiO: The $^3\Sigma^-$ ground state, J. Chem. Phys., 89, 2748–2753, doi:10.1063/1.455711, 1988.
Sternberg, J. R. and Ingham, M. F.: Observations of the airglow continuum, Mon. Not. Roy. Astr. Soc., 159, 1–20, 1972.
Watson, L. R., Thiem, T. L., Dressler, R. A., Salter, R. H., and Murad, E.: High temperature mass spectrometric studies of the bond energies of gas-phase zinc oxide, nickel oxide, and copper(II) oxide, J. Phys. Chem., 97(21), 5577–5580, doi:10.1021/j100123a020, 1993.
West, J. B. and Broida, H. P.: Chemiluminescence and photoluminescence of diatomic iron oxide, J. Chem. Phys., 62, 2566–2574, 1975.

ACPD
11, 11839–11859, 2011

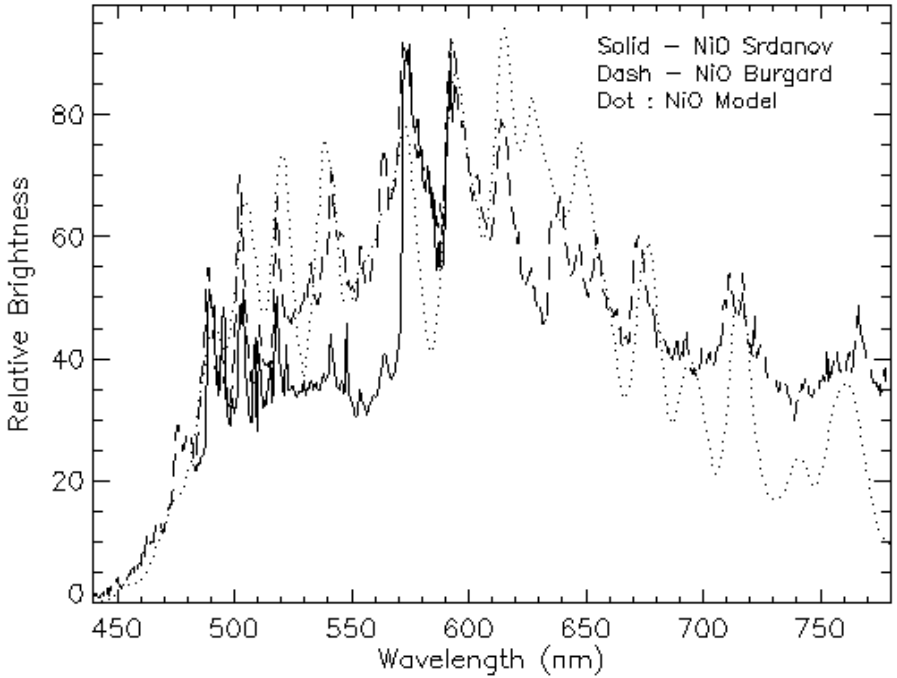

Fig. 1. A comparison of two laboratory spectra of chemiluminescent NiO^* together with a preliminary spectral model simulation. The resolution of the Burgard spectrum in the visible region is approximately 6 nm.

ACPD
11, 11839–11859, 2011

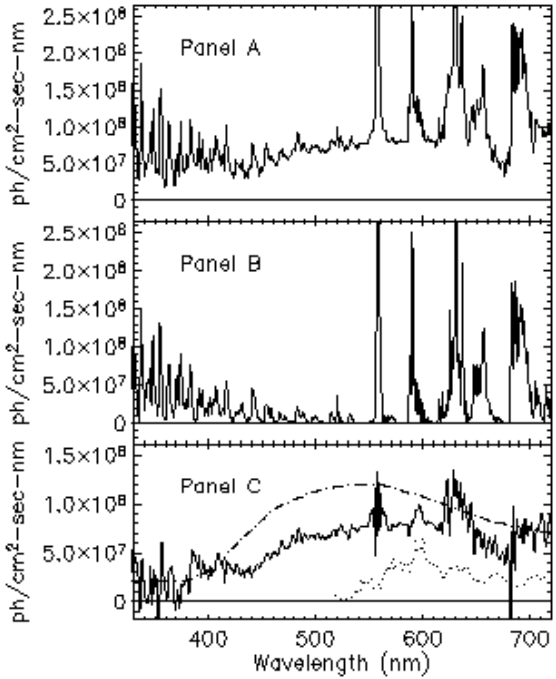

Fig. 2. **(A)** Averaged night airglow limb spectrum from the Arizona GLO-1 spectrograph onboard STS 53. **(B)** Simulated night airglow spectrum to match the known spectral features in **(A)**. **(C)** Panel **(A)** observed spectrum minus panel **(B)** model spectrum. The observed difference spectrum is spectrally convolved with a 1.3 nm half width triangular function to improve figure clarity. Narrow spectral artifacts remain at the locations of the bright airglow atomic lines. The residual is a 'continuum' with a broad peak near 600 nm. The NO + O → NO* chemiluminescent spectrum (Gattinger et al., 2009) is shown in **(C)** (dot-dash) for comparison. Similarly, the mesospheric model FeO* chemiluminescent spectrum (Gattinger et al., 2011) is shown in **(C)** (dot) for reference.

ACPD
11, 11839–11859, 2011

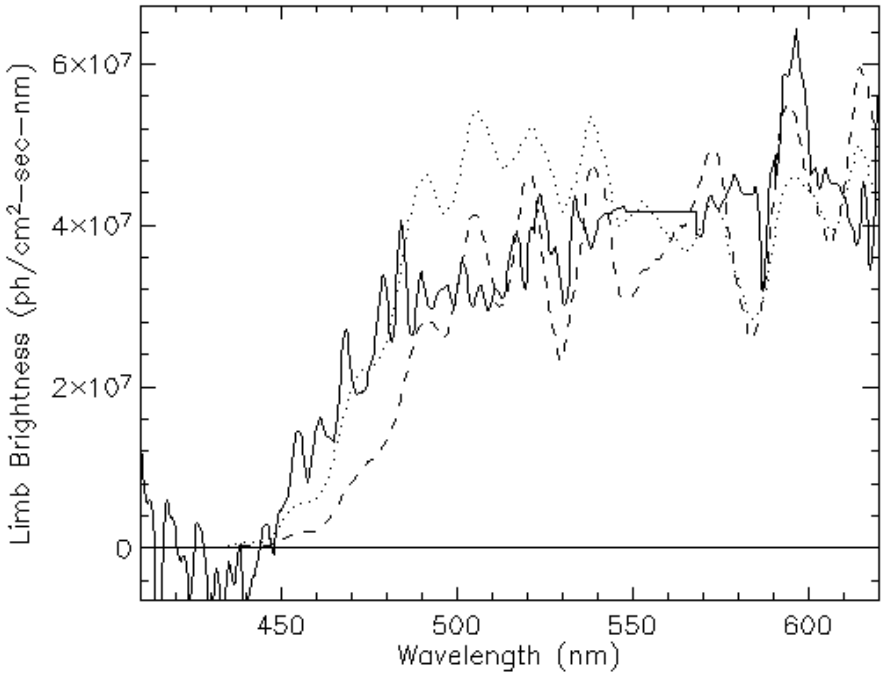

Fig. 3. Comparison between the GLO-1 observed airglow limb "continuum" (solid, from Panel C of Fig. 2) and the NiO* model spectra for laboratory pressure (dash, from Fig. 1) and for mesospheric pressure (dot). The large noise spikes in the difference spectrum at OI 558 nm (Panel C of Fig. 2) are replaced by a straight line.

ACPD
11, 11839–11859, 2011

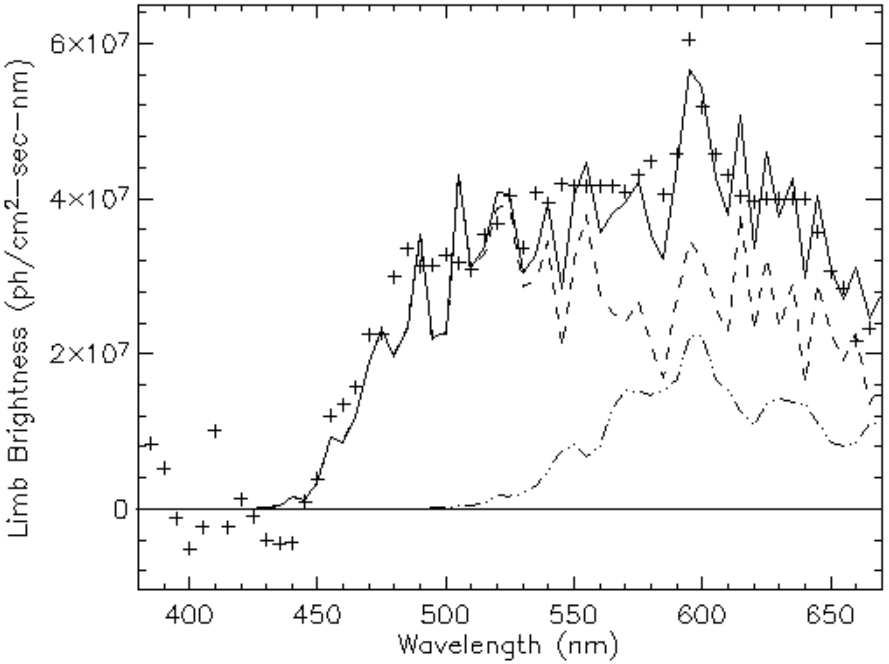

Fig. 4. A least-squares fit of the chemiluminescent FeO^* model spectrum (dot-dot-dash) and NiO^* model spectrum (dash) with the GLO-1 observed airglow limb "continuum" from Panel C of Fig. 2 (+ + +), all averaged over 5 nm intervals. The large noise spikes in the difference spectrum at OI 558 nm and OI 633 (Panel C of Fig. 2) are replaced by straight lines. The ratio of NiO^* to FeO^* is 3.2 ± 0.4 integrated over the full spectral range of Fig. 4.

ACPD
11, 11839–11859, 2011

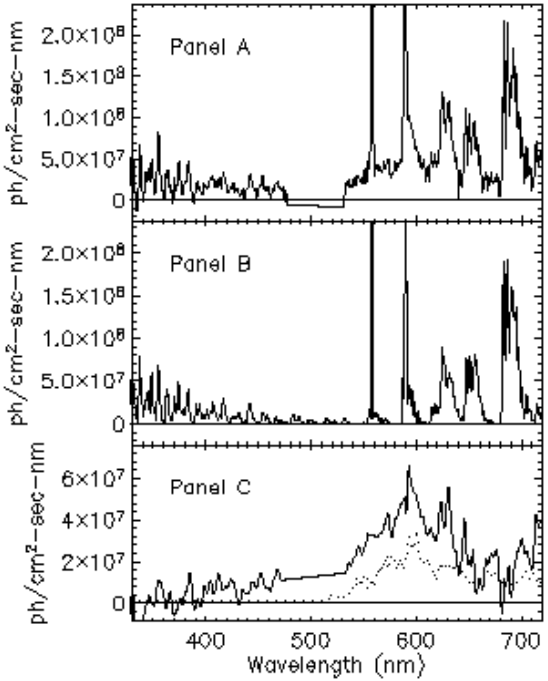

Fig. 5. (A) OSIRIS averaged tangent limb spectrum for June and July of 2004. The gap from 480 nm to 530 nm is the location of the OSIRIS spectral order sorter. **(B)** Simulated night airglow spectrum scaled to match Panel A observed spectral features. **(C)** Residual spectrum (**A** minus **B**). The observed difference spectrum is spectrally convolved with a 2.5 nm half width triangular function to improve figure clarity. The data gap from 480 nm to 530 nm in **(C)** is filled assuming linear interpolation, and similarly for the strong OI 558 nm region . The model FeO^* chemiluminescent spectrum (Gattinger et al., 2011) is shown in **(C)** (dot) for comparison.

ACPD
11, 11839–11859, 2011

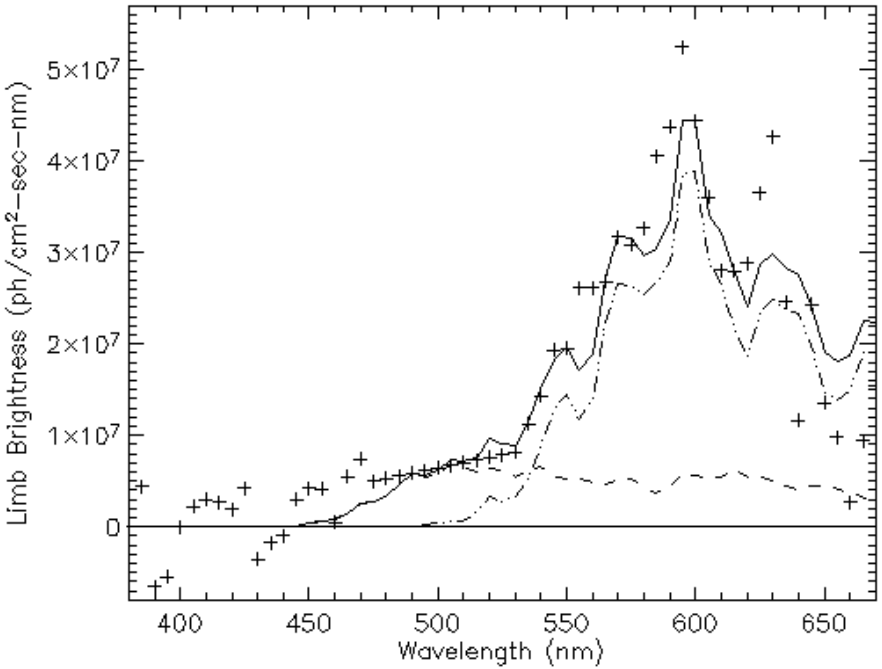

Fig. 6. A least-squares fitting of the chemiluminescent FeO^* model spectrum (dot-dot-dash) and NiO^* model spectrum (dash) to the OSIRIS observed airglow limb "continuum" from Panel C of Fig. 5 (+ + +), all averaged over 5 nm intervals. The ratio of NiO^* to FeO^* is 0.3 ± 0.1 integrated over the full spectral range of Fig. 6.

ACPD
11, 11839–11859, 2011